

# On the use of adaptive gridding methods for modelling chemical transport from multi-scale sources

A.Tomlin\*, M.Berzins, J. Ware, J. Smith, M.J. Pilling  
Department of Fuel and Energy, School of Computer Studies  
and School of Chemistry  
University of Leeds  
Leeds LS2 9JT  
UK

October 5, 2011

## Abstract

This paper investigates the solution of atmospheric reaction/flow problems using time-dependent adaptive mesh gridding techniques. Preliminary studies of time varying problems in two space dimensions related to the effects of power station emissions on regional ozone levels have been carried out. The results show the importance of using adaptive grids in order to represent the interaction of the plume with background air over large distances. The adaptive mesh reveals features of cross wind concentration profiles which would not be shown using the standard mesh sizes adopted in regional atmospheric calculations. As the level of adaptivity increases, and the mesh becomes locally refined in regions of large spatial error, the total and peak ozone concentrations change quite significantly. The results demonstrate that the level of error which can result from using fixed or telescopic grid approaches for spatially inhomogeneous source patterns may be significantly reduced by the use of adaptive meshes.

## 1 Introduction

Computational models describing the chemical transformations and transport of species in the troposphere have an essential role in understanding the complex processes which lead to the formation of pollutants such as greenhouse gases, acid rain and photochemical oxidants. As such they have an important bearing on predicting future effects of emissions on for example radiative forcing, and on the health of animal and plant life. An accurate and detailed description of the distribution of pollutant concentrations is needed over large

spatial regions in order to compare with field measurement calculations. Such comparisons are usually made at fixed points and therefore high resolution models will inevitably promote a better understanding of the processes which lead to high concentrations in certain areas. One of the key issues which has to be addressed is the long range interaction between different emission sources. It is necessary to understand the mixing between plumes generated from concentrated sources and distributed urban and biogenic emissions or background concentrations in order to formulate abatement strategies.

Achieving high resolution in air pollution models is a difficult challenge because of the large number of species present in the atmosphere. The number of chemical rate equations which need to be solved rises with the number of species, and for high resolution 3-dimensional calculations, detailed chemical schemes can become prohibitively large. The range of reaction time-scales can lead to stiff systems of differential equations which require more expensive numerical solvers. In order to address the computational problems posed by complex atmospheric problems previous models have adopted two strategies.

The first strategy has been to retain the detailed chemistry necessary for understanding the many reactions of pollutants such as NO<sub>x</sub>, SO<sub>2</sub> and volatile organic compounds, and to use 1-D trajectory models or coarse Eulerian grid models to simulate the reaction/transport problem (Derwent et al,1990). Such models have been essential in developing an understanding of how chemical species interact to form secondary pollutants such as ozone. They have not, however, provided the spatial resolution which is needed to understand the complex interaction between multiple sources of both concentrated and distributed types. They also require an oversimplification of the mixing processes which can occur between plumes from these sources.

The second approach has been to use a simplified chemical model but with a high resolution grid. In this case problems arise in assessing the role of individual species on the pollutant distribution. In order to achieve high spatial resolution, and chemical accuracy a new modelling strategy is required.

It has been recognised that new approaches to achieving accuracy are necessary and some steps have been taken in regional air quality models to include the use of variable sized grids, thus achieving better resolution in some regions. A recent review paper by Peters et al. (1995) highlights the importance of developing more efficient grid systems for the next generation of air pollution models in order to “capture important smaller scale atmospheric phenomena”. Grid refinement in these telescopic models has been used in a prescribed way (Moussiopoulous,1994, Jakobs et al, 1994, Sunderam et al, 1990, Sillman et al, 1990). This allows for refinement in, for example, high emission areas, but cannot take account of the spatial gradients resulting from the dispersion of pollutants through the atmosphere. Away from concentrated sources such models use large grids of up to 50 kilometres. Since dispersion can carry species distances of hundreds of kilometres from the source, such prescribed telescopic gridding models could still lead to inaccurate downwind profiles as the plumes travel into those areas with larger grids. This is a particular problem when modelling species such as ozone, where the chemical time-scale of pollutant formation is such that the main pollution episodes occur at very long distances downwind of the sources of photochemical

precursors. The regions of steep spatial gradients of species such as ozone will move with time according to the wind-field present and the spatial distribution of emissions. A reliable solution can only be obtained if the mesh can refine accordingly. The fine scale grids used in present regional scale models are of the order of 10-20km. For a power plant plume with a width of approximately 20km, it is impossible to resolve the fine structure within the plume using grids of this size. Furthermore, to refine the mesh a priori, according to the path of the plume, would be an impossible task since the plume position is a complicated function of many factors, including reaction, deposition and transport. There is a need for the application of methods which can refine the grid according to where the solution requires it i.e. time-dependent adaptive algorithms.

More recently there have been some applications of adaptive grids for environmental modelling, e.g Skamarock et. al. (1989), although as yet these methods have not been implemented in standard air quality models. The present work describes how adaptive gridding techniques, which automatically refine the mesh in regions of high spatial error, can improve on the telescopic approach. The aim of this work is to show that the use of such techniques will lead to a better understanding of the complex multiscale phenomena that arise from regional scale models. In this paper we have not attempted to develop a comprehensive regional model, but rather to apply a set of numerical modelling tools to particular test cases in order to demonstrate their advantages over traditional techniques. The test cases we have chosen are firstly the standard linear advection problem of Molenkamp (1968), which serves to demonstrate that the numerical scheme chosen is suitable for atmospheric dispersion, and secondly the interaction of a power plant plume with background emissions.

A power plant plume is a highly concentrated source of NO<sub>x</sub> emissions which can be carried through the atmosphere for hundreds of kilometres, and so provides a stringent test of whether adaptive gridding methods can lead to more reliable results for complex multi-scale models. Since power stations provide some of the highest emission sources for NO<sub>x</sub> it is important to be able to generate an accurate understanding of their impact not only on the total NO<sub>x</sub> budget, but also on the generation of secondary pollutants such as ozone. To achieve this we must consider the interaction of the plume with its surroundings, and in the model we look at background scenarios of both clean and polluted air (Tomlin et al, 1994). The test case model covers a region of 300 x 500 km. To keep the model simple, and therefore reveal particular issues related to the mesh, we have used a reduced chemical scheme with idealised dispersion conditions. The domain is approximated by an unstructured triangular mesh which can then be adapted to higher and higher levels of refinement according to errors in solution components. The solution technique is based on the spatial discretisation of a set of advection/diffusion equations on the unstructured mesh using a finite volume, flux limited scheme. The aim throughout the paper is to demonstrate the potential of a particular methodology for use in future atmospheric models rather than to use a well tested model to study a real life situation. The simplified model will be used to illustrate how grid resolution can affect the solution of nonlinear chemical transport problems and how new features of the cross plume concentration profile can be revealed by the adaptive solution, This will be achieved by comparison of results from the adaptive mesh with those from a base mesh of the order commonly found in regional scale models.

The paper is structured as follows. In Section 2 we briefly introduce the form of the equations which describe atmospheric reaction flow problems. In Sections 3 and 4 we describe the numerical scheme we have used to solve these equations for the two test cases. In Section 3, a description of the use of unstructured triangular meshes and the spatial discretisation scheme will be given. In section 4 we discuss the method adopted for time integration. In Section 5 the methods used for the initial mesh generation and the criteria used for mesh refinement are introduced. In Sections 6 and 7 the two test cases are described. The first is a simple 2D linear advection problem with no source terms. This case illustrates the accuracy of low and high order schemes for convection dominated problems. The second problem relates to the dispersion and reaction of NOx emissions from a power station source. This is a multiscale problem coupling chemistry and flow of the type found in regional air pollution models. Finally in Sections 8 and 9 we present a discussion and conclusions about the use of adaptive methods in air pollution models.

## 2 Model equations

The atmospheric diffusion equation in two space dimensions is given by:

$$\begin{aligned} \frac{\partial c_s}{\partial t} = & -\frac{\partial(uc_s)}{\partial x} - \frac{\partial(wc_s)}{\partial y} + \frac{\partial}{\partial x} \left( K_x \frac{\partial c_s}{\partial x} \right) + \frac{\partial}{\partial y} \left( K_y \frac{\partial c_s}{\partial y} \right) \\ & + R_s(c_1, c_2, \dots, c_q) + E_s - (\kappa_{1s} + \kappa_{2s})c_s, \end{aligned} \quad (1)$$

where  $c_s$  is the concentration of the  $s$ 'th compound,  $u, w$ , are horizontal wind velocities,  $K_x$  and  $K_y$  are turbulent diffusivity coefficients and  $\kappa_{1s}$  and  $\kappa_{2s}$  are dry and wet deposition velocities respectively.  $E_s$  describes the distribution of emission sources for the  $s$ 'th compound and  $R_s$  is the chemical reaction term which may contain nonlinear terms in  $c_s$ . For  $n$  chemical species an  $n$ -dimensional set of partial differential equations (p.d.e.s) is formed describing the rates of change of species concentration over time and space, where each is coupled through the nonlinear chemical reaction terms.

The restriction to two space dimensions has the advantage that the present study will be able to concentrate on showing that standard adaptive numerical methods have the potential to reveal detail not previously observed in plume models. In this sense the work described here is a necessary precursor to the development of a full 3D code for such problems.

## 3 Triangular Finite Volume Method.

The basis of the numerical method is the space discretisation of the p.d.e.s derived from the atmospheric diffusion equation on unstructured triangular meshes using the software SPRINT2D (Berzins et al, 1992, 1997). This approach, (known as the "Method of Lines"),

reduces the set of p.d.e.s in three independent variables to a system of ordinary differential equations (o.d.e.s) in one independent variable, time. The system of o.d.e.s can then be solved as an initial value problem, and a variety of powerful software tools exist for this purpose (Berzins et al, 1989). For advection dominated problems it is important to choose a discretisation scheme which preserves the physical range of the solution. A more in-depth discussion of the methods can be found in references (Berzins et al, 1989, 1992, 1994a,1994b,1995).

Unstructured triangular meshes are popular with finite volume/element practitioners because of their ability to deal with general two-dimensional geometries. In terms of application to multi-scale atmospheric problems, we are not dealing with complex physical geometries, but unstructured meshes provide a good method of resolving the complex structures formed by the interaction of chemistry and flow in the atmosphere and by the varying types of emission sources. The term unstructured represents the fact that each node in the mesh may be surrounded by any number of triangles whereas in a structured mesh this number would be fixed. The discretisation of advection/diffusion/reaction equations on unstructured meshes will now be discussed.

For systems of equations such as (1) it is useful to consider the advective and diffusive fluxes separately in terms of the discretisation. In the present work, a flux limited, cell-centered, finite volume discretization scheme of Berzins and Ware (1994,1995) was chosen. This method enables accurate solutions to be determined for both smooth and discontinuous flows by making use of the local Riemann solver flux techniques (originally developed for the Euler equations) for the advective parts of the fluxes, and centered schemes for the diffusive part. The scheme used for the treatment of the advective terms is an extension to irregular triangular meshes of the nonlinear scheme described by Spekreijse (1987) for regular Cartesian meshes. The scheme of Berzins and Ware has the desirable properties, see Chock (1991), of preserving positivity eliminating spurious oscillations and restricting the amount of diffusion by the use of a nonlinear limiter function. Recent surveys of methods for the advection equation (VanLoon, 1996, Vreugdenhil and Koren, 1993) have suggested the use of a very similar scheme to Spekreijse for regular Cartesian meshes, preferring it to schemes such as Flux Corrected Transport.

To illustrate this method, consider the advection-reaction equation:

$$\frac{\partial c}{\partial t} = -\frac{\partial uc}{\partial x} - \frac{\partial wc}{\partial y} + R(c) \quad , t \in (0, t_e) \quad , (x, y) \in \Omega \quad (2)$$

with appropriate boundary and initial conditions. A finite volume type approach is adopted in which the solution value at the centroid of triangle  $i$ ,  $(x_i, y_i)$ , is  $c_i$  and the solutions at the centroids of the triangles surrounding triangle  $i$  are  $c_l$ ,  $c_j$  and  $c_k$ . Integration of equation (2) on the  $i$ th triangle, which has area  $A_i$ , use of the divergence theorem, and the evaluation of the line integral along each edge by the midpoint quadrature rule gives an o.d.e. in time:

$$\frac{dc_i}{dt} = -\frac{1}{A_i}(uc_{ik}\Delta y_{0,1} - vc_{ik}\Delta x_{0,1} + uc_{ij}\Delta y_{1,2} - vc_{ij}\Delta x_{1,2} + uc_{il}\Delta y_{2,0} - vc_{il}\Delta x_{2,0}) + R(c_i), \quad (3)$$

where  $\Delta x_{ij} = x_j - x_i$ ,  $\Delta y_{ij} = y_j - y_i$ . The fluxes  $uc_{ij}$  and  $vc_{ij}$  in the  $x$  and  $y$  directions respectively are evaluated at the midpoint of the triangle edge separating the triangles associated with  $c_i$  and  $c_j$ . These fluxes are evaluated by taking account of the flow directions with respect to the orientation of the triangle. This is achieved by using either the *left* or *right* solution values depending on the direction of advection and how each edge is aligned. These *left* and *right* solution values for each edge in a triangle are defined as the *left* solution value being that internal to the  $i$ th triangle, and the *right* solution value being that external to triangle  $i$ . Consider for example the case shown in Figure (1) when  $u$  is positive and  $x_i < x_j$  this means that the  $x$  component of the advection is blowing from node  $i$  to node  $j$ , and so  $c_{ij} = c_{ij}^l$ . Similarly when  $v$  is positive the  $y$  component of the wind is blowing from node  $k$  to node  $i$  and so  $c_{ik} = c_{ik}^r$ . Hence, equation (3) may be written as

$$\frac{dc_i}{dt} = -\frac{1}{A_i}(uc_{ik}^l\Delta y_{0,1} - vc_{ik}^r\Delta x_{0,1} + uc_{ij}^l\Delta y_{1,2} - vc_{ij}^l\Delta x_{1,2} + uc_{il}^r\Delta y_{2,0} - vc_{il}^l\Delta x_{2,0}) + R(c_i), \quad (4)$$

A simple first-order scheme uses  $c_{ij}^l = c_i$ ,  $c_{ij}^r = c_j$  on the edge between triangles  $i$  and  $j$ . This scheme is very diffusive and so Berzins and Ware (1995) use a complex interpolation scheme to obtain the *left* and *right* values on each edge. The interpolants in this second order scheme, use a constrained or limited form of the solution obtained from the six triangles surrounding an edge giving a ten triangle stencil for the discretization of the convective terms on each triangle.

For example, the value  $c_{ij}^l$  is constructed by forming a linear interpolant using the solution values  $c_i$ ,  $c_k$  and  $c_l$  at the three centroids. An alternative interpretation is that linear extrapolation is being used based on the solution value  $c_i$  and an intermediate solution value (itself calculated by linear interpolation)  $c_{lk}$  which lies on the line joining the centroids at which  $c_l$  and  $c_k$  are defined (see Figure 1) i.e.

$$c_{ij}^l = c_i + \Phi(S_{ij}) d_{ij,i} \frac{c_i - c_{lk}}{d_{i,lk}}, \quad (5)$$

where the argument  $S$  is a ratio of solution gradients, see Berzins and Ware (1995) and the generic term  $d_{a,b}$  denotes the positive distance between points  $a$  and  $b$ . For example  $d_{ij,i}$  denotes the positive distance between points  $ij$  and  $i$ , see Figure 1, as defined by

$$d_{i,ij} = \sqrt{(x_i - x_{ij})^2 + (y_i - y_{ij})^2}, \quad (6)$$

where  $(x_{ij}, y_{ij})$  are the co-ordinates of  $c_{ij}$ . In order to preserve positivity in the numerical solution, the limiter function  $\Phi$  is used and has to satisfy  $\Phi(S)/S \leq 1$ , see Berzins and Ware (1995). These conditions are satisfied, for example, by a modified van Leer limiter defined by:

$$\Phi(S) = (S + |S|)/(1 + \text{Max}(1, |S|)) . \quad (7)$$

The value  $c_{ij}^r$  is defined in a similar way using the centroid values  $c_j$ ,  $c_s$  and  $c_r$ . This scheme is of second order accuracy, see Berzins and Ware (1995). The diffusion terms are discretised by using a finite volume approach to reduce the integrals of second derivatives

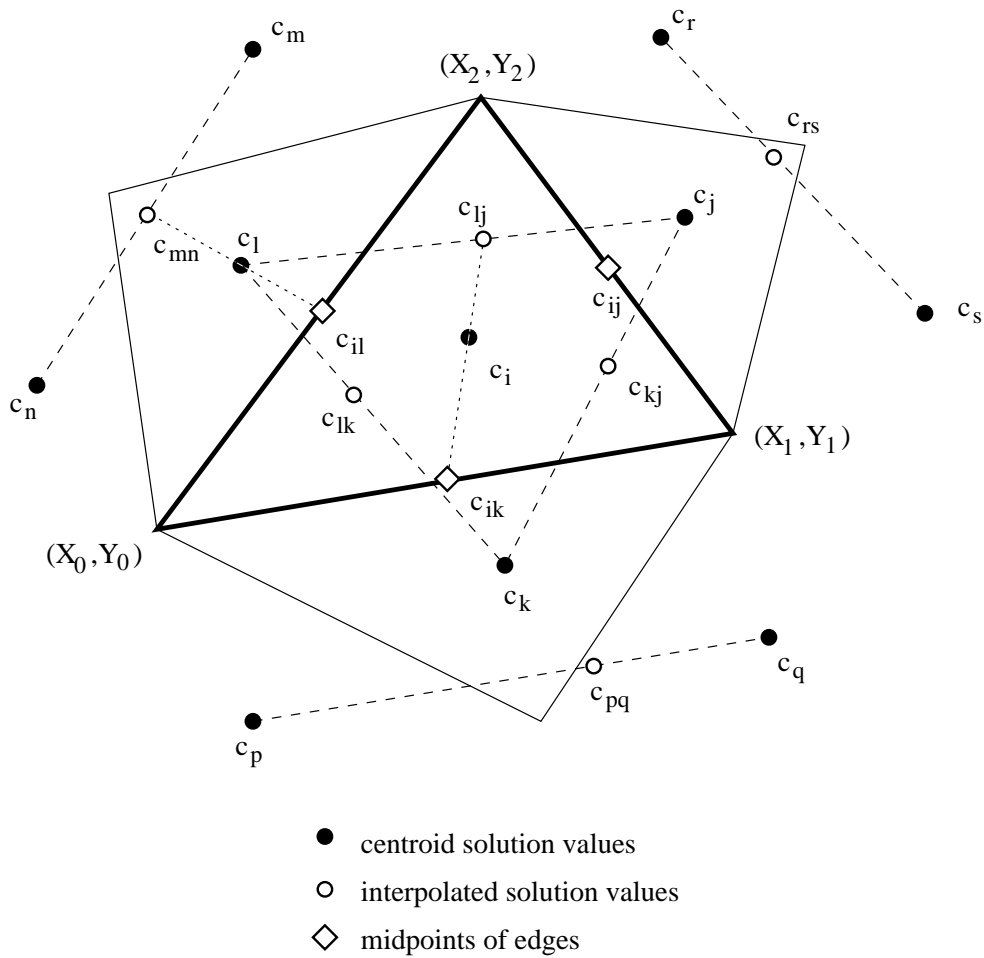


Figure 1: Construction of interpolants used in the calculation of fluxes for the irregular mesh.

to the evaluation of first derivatives at the midpoints of edges. These first derivatives are then evaluated by differentiating a bilinear interpolant based on four mid-point values, see Berzins and Ware (1994). The boundary conditions are implemented by including them in the definitions of the advective and diffusive fluxes at the boundary.

## 4 Time Integration.

A method of lines approach with the above spatial discretization scheme results in a system of o.d.e.s in time which are integrated using the code SPRINT (Berzins et al, 1989) with the Theta option which is specially designed for the solution of stiff systems with moderate accuracy and automatic control of the local error in time. Once the p.d.e.s have been discretised in space we are left with a large system of coupled o.d.e.s of dimension  $m \times n$  where  $m$  is the number of triangles in the mesh, and  $n$  the number of species. These equations may now be written as

$$\dot{\underline{c}} = \underline{F}_N ( t, \underline{c}(t) ) , \quad \underline{c}(0) \text{ given} , \quad (8)$$

where the vector,  $\underline{c}(t)$ , is defined by  $\underline{c}(t) = [c(x_1, y_1, t), \dots, c(x_N, y_N, t)]^T$ . The point  $x_i, y_i$  is the centre of the  $i$  th cell and  $C_i(t)$  is defined as a numerical approximation to the exact solution to the p.d.e. evaluated at the centroid i.e.  $c(x_i, y_i, t)$ . The method of lines approach is used to numerically integrate equation (8) thus generating an approximation,  $\underline{C}(t)$ , to the vector of exact p.d.e. solution values at the mesh points,  $\underline{c}(t)$ .

The Theta method (Berzins and Ware, 1995, Berzins, 1994), which has been used for the experiments described here, defines the numerical solution at  $t_{n+1} = t_n + k$ , where  $k$  is the time step size, as denoted by  $\underline{C}(t_{n+1})$ , by:

$$\underline{C}(t_{n+1}) = \underline{C}(t_n) + (1 - \theta)k \dot{\underline{C}}(t_n) + \theta k \underline{F}_N(t_{n+1}, \underline{C}(t_{n+1})), \quad (9)$$

in which  $\underline{C}(t_n)$  and  $\dot{\underline{C}}(t_n)$  are the numerical solution and its time derivative at the previous time  $t_n$  and  $\theta = 0.55$ . This system of equations is solved by either using functional iteration or a Newton Krylov method. If the latter method is used the equations leading to the correction of the solution  $\underline{\Delta C}$  for the  $p + 1$  th iteration of the modified Newton iteration used with the Theta method are:

$$[I - k\theta J] \underline{\Delta C} = \underline{r}(t_{n+1}^p) \quad (10)$$

where

$$\begin{aligned} \underline{r}(t_{n+1}^p) &= -\underline{C}(t_{n+1}^p) + \underline{C}(t_n) + (1 - \theta)k\dot{\underline{C}}(t_n) - \theta k \underline{F}_N(t_{n+1}, \underline{C}(t_{n+1}^p)), \\ J &= \frac{\partial \underline{F}_N}{\partial \underline{C}}, \quad \text{and} \quad \underline{\Delta C} = [\underline{C}(t_{n+1}^{p+1}) - \underline{C}(t_{n+1}^p)]. \end{aligned} \quad (11)$$

The solution of this system of equations constitutes the major computational task of a method of lines calculation. In cases where large o.d.e. systems result from the discretization of flow problems with complex chemistry (50,000 equations typically), the c.p.u. times seem to be excessive.

## 4.1 Operator Splitting.

One approach which overcomes the problem of excessive computational time is to use a form of operator splitting based on a decomposition of the p.d.e.s into a set of flow terms and a source reactive term. Consider the o.d.e. function  $\underline{F}_N(t, \underline{c}(t))$  defined by equation (8) and decompose it into two parts:

$$\underline{F}_N(t, \underline{c}(t)) = \underline{F}_N^f(t, \underline{c}(t)) + \underline{F}_N^s(t, \underline{c}(t)) \quad (12)$$

where  $\underline{F}_N^f(t, \underline{c}(t))$  represents the discretization of the convective flux terms  $f$  and  $g$  in equation (1) and  $\underline{F}_N^s(t, \underline{c}(t))$  represents the discretization of the source term  $h$  in the same equation. The splitting approach used, (Berzins and Ware, 1996), is to employ the following approximation to the Jacobian matrix used by the Theta method within the Newton iteration defined by equation (10):

$$I - k\theta J \approx [I - k\theta J_f] [I - k\theta J_s] + O(k^2). \quad (13)$$

where

$$J_f = \frac{\partial \underline{F}_N^f}{\partial \underline{c}}, \quad J_s = \frac{\partial \underline{F}_N^s}{\partial \underline{c}}.$$

The matrix  $I - k\theta J_s$  is thus those parts of the Jacobian matrix in equation (10) which correspond to the discretization of the time derivatives and the source terms in the vector  $\underline{h}$ . The disadvantage of this approach is that it introduces a second-order splitting error. Fortunately this error only alters the rate of convergence of the iteration as the residual being reduced is still that of the full o.d.e. system.

This matrix is thus block-diagonal with as many block as there are triangles and with each block having as many rows and columns as there are p.d.e.s. The fact that the blocks relate only to the chemistry plus source/sink terms within each cell, means that each block may be inverted (or the equations may be solved) independently using LU decomposition. This approach may also be interpreted as approximating the flow term  $[I - k\theta J_f]$  by the identity matrix, as is done when using functional iteration with the Theta method applied to flow alone (Berzins, 1994). Since the spatial discretization method connects each triangle to as many as ten others it follows that the matrix  $[I - k\theta J_f]$  may have a much more complex sparsity pattern than that of the matrix  $[I - k\theta J_s]$ . Approximating the matrix  $[I - k\theta J_f]$  by the identity matrix (Berzins and Ware, 1996) thus eliminates a large number of the full Jacobian entries.

The new operator-splitting iteration may thus be written as

$$[I - k\theta J_s] \underline{\Delta C}^* = \underline{r}(t_{n+1}^p) \quad (14)$$

where  $\underline{\Delta C}^*$  is the operator splitting approximation to  $\underline{\Delta C}$ . The advantage of this is that a form of functional iteration may be used to solve the nonlinear equations provided that the residuals on each triangle are multiplied by the inverse of the matrix  $I - k\theta J_s$ , (or the equivalent linear systems solved). This modified form of functional iteration has been

implemented as a new linear algebra module inside the SPRINT2D software and has been found to give increases in speed-up by a factor of between five and ten over using a Newton-Krylov method. Further increases in speed are possible by using iterative methods such as those suggested by Verwer (1994) to solve the system of equations (14) on a block by block basis.

The disadvantage of introducing operator splitting is that it is difficult to evaluate the resulting error. As the splitting is only used to speed up the solution of the nonlinear equations, and providing that the iteration is continued until the residual  $\underline{r}(t_{n+1}^p)$  is sufficiently small, this error does not have the same impact as introducing splitting at the p.d.e. level. It is however possible to obtain a rough idea of the splitting error on each iteration. In order for the operator-splitting iteration defined by equation (13) to converge with a rate of convergence  $r_c$  it is necessary, (Berzins and Ware, 1996), that

$$\| [I - k\theta J_s]^{-1} k \theta J_f \| < r_c$$

where  $r_c < 1$ . In contrast, the convergence condition when functional iteration is used and no chemistry is present is:

$$\| k \theta J_f \| < r_c$$

Berzins and Ware (1995) show that a CFL-like condition is satisfied if functional iteration converges quickly. Hence, in the case when the term  $J_s$  may have large negative eigenvalues e.g for fast chemistry, the new operator splitting iteration may act to increase the size of stable timesteps over the case when flow alone is involved. Not every component will necessarily be affected by such eigenvalues and so it is still necessary to consider the stable stepsize for the flow alone.

## 4.2 Stability and Time Error Control.

The topic of choosing a stable stepsize for the finite volume method has been considered in detail by Berzins and Ware (1995, Ware and Berzins, 1995). In the case of the first order method with the limiter function defined in equation (7) set to zero they showed that for the p.d.e. of the form of equation (2) with  $R(c) = 0$ , if  $L_i$  is the length of the longest edge of the triangle  $i$ , a sufficient condition for stability and hence positivity is,

$$k_n \frac{L_i}{A_i} (u + v) \leq \frac{1}{\theta m}. \quad (15)$$

where  $A_i$  is the area of triangle  $i$ ,  $u$  and  $v$  are as defined in equation (1) and  $m$  is the number of functional iterations. This is a CFL type stability condition that depends on the term  $L_i/A_i$  which is also used as a measure of the *quality* of a triangle. Although only one possible alignment to the characteristic directions has been considered, similar results are produced by considering the other possibilities.

In the case when a limiter function is used this result has been extended to arrive at the stability condition

$$(1 + 2d_{max}) k_n \frac{L_i}{A_i} (u + v) \leq \frac{1}{\theta m}. \quad (16)$$

where  $d_{max}$  is the maximum value of the ratio of distances such as  $d_{ij,i}/d_{i,lk}$  used in equation (5) and where from equation (7)  $0 \leq \Phi(.) \leq 2$ .

Although a CFL condition indicates when the underlying flow without reactions is stable, it is still necessary to get the required accuracy for the chemistry terms. In most time dependent p.d.e. codes either a CFL stability control is employed or a standard o.d.e. solver is used which controls the local error  $L_{n+1}(t_{n+1})$  with respect to a user supplied accuracy tolerance. Efficient time integration requires that the spatial and temporal errors are roughly the same order of magnitude. The need for spatial error estimates unpolluted by temporal error, requires that the spatial error is the larger of the two. Although one way of achieving this might be to extend the approach of Berzins (1994) which controls the local time error to be a fraction of the growth in the spatial discretization error over a timestep. We shall adopt a standard local error approach given by:

$$\| L_{n+1}(t_{n+1}) \| < TOL. \tag{17}$$

## 5 Mesh Generation and Adaptivity.

The initial unstructured meshes used in SPRINT2D are created from a geometry description using the Geompack (Joe and Simpson, 1991) mesh generator. These meshes are then refined and coarsened by the Triad adaptivity module which uses data structures to enable efficient mesh adaptation.

Since the initial mesh is unstructured we have to be very careful in choosing the data structure which provides the necessary information for refining and derefining the mesh. When using a structured mesh it is possible to number mesh vertices or elements explicitly. This is not possible for unstructured meshes and therefore the data structure must provide the necessary connectivity. The important factor is to maintain the quality of the triangle as the mesh is refined and coarsened. This is achieved using a tree-like data structure with a method of refinement based on the regular subdivision of triangles. Here an original triangle is split into four similar triangles by connecting the midpoints of the edges as shown in Figure 2. These may later be coalesced into the parent triangle when coarsening the mesh. This process is called local h-refinement, since the nodes of the original mesh do not move and we are simply subdividing the original elements. Similar procedures are extensively used with a wide range of both finite element and volume methods for a very broad range of physical problems.

Once a method of refinement and derefinement has been implemented, it remains to decide on a suitable criterion for the application of the adaptivity. The ideal situation would be that the decision to refine or derefine would be made on a fully automatic basis with no user input necessary. In practice a combination of an automatic technique and some knowledge of the physical properties of the system is used. The technique used in this work is based on the calculation of spatial error estimates. Low and high order solutions are obtained and the difference between them gives the spatial error, see Berzins (1995). The algorithm can then choose to refine in regions of high spatial error by comparison with a user defined tolerance.

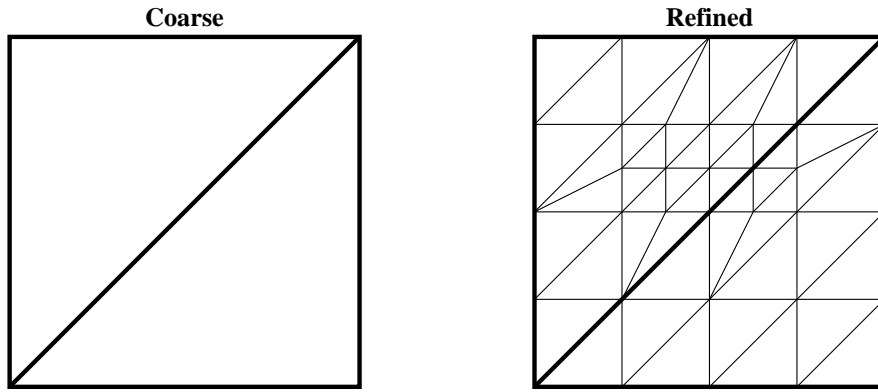


Figure 2: Method of local refinement based on the subdivision of triangles

For the  $i$ th p.d.e. component on the  $j$ th triangle, a local error estimate  $e_{i,j}(t)$  is calculated from the difference between the solution using a first order method and that using a second order method. For time dependent p.d.e.s this estimate shows how the spatial error grows locally over a time step. A refinement indicator for the  $j$ th triangle is defined by an average scaled error ( $serr_j$ ) measurement over all  $npde$  p.d.e.s using supplied absolute and relative tolerances:

$$serr_j = \sum_{i=1}^{npde} \frac{e_{i,j}(t)}{atol_i/A_j + rtol_i \times C_{i,j}}, \quad (18)$$

where  $atol$  and  $rtol$  are the absolute and relative error tolerances. This formulation for the scaled error provides a flexible way to weight the refinement towards any p.d.e. error. An integer refinement level indicator is calculated from this scaled error to give the number of times the triangle should be refined or derefined. Since the error estimate is applied at the end of a time-step it is too late to make the refinement decision. Methods are therefore used for the prediction of the growth of the spatial error using linear or quadratic interpolants. The decision about whether to refine a triangle is based on these predictions, and the estimate made at the end of the time-step can be used to predict errors at future time-steps. Generally it is found that large spatial errors coincide with regions of steep spatial gradients. The spatial error estimate can also be used to indicate when the solution is being solved too accurately and can indicate which regions can be coarsened. The tree data structure can then be used to restore a lower level mesh which maintains the triangle quality.

For applications such as atmospheric modelling it is important that a maximum level of refinement can be set, to prevent the code from adapting to too high a level in regions with concentrated emissions. This is especially important around point or highly concentrated area sources. Here, because of the nature of the source, steep spatial gradients are likely to persist down to very high levels of refinement. This would have the consequence that the number of elements on which the p.d.e.s had to be discretised would become prohibitively large. For the following test problems the maximum level of refinement was therefore limited to level 3. The actual size of the mesh elements used at each computational step will depend on the size of elements in the initial mesh and on the maximum level of refinement.

## 6 Molenkamp Linear Advection Test Problem

The first test case studied was the classical linear advection equation, of Molenkamp (1968).

$$\frac{\partial c}{\partial t} = -\pi \left( y - \frac{1}{2} \right) \frac{\partial c}{\partial x} - \pi \left( x - \frac{1}{2} \right) \frac{\partial c}{\partial y} \quad (19)$$

The solution domain is the circle,

$$\left( x - \frac{1}{2} \right)^2 + \left( y - \frac{1}{2} \right)^2 < 2.$$

The initial conditions describe a peak with centre at (0.5,0.75),

$$c(x, y, 0) = \exp \left( -80 \left[ \left( x - \frac{1}{2} \right)^2 + \left( y - \frac{3}{4} \right)^2 \right] \right). \quad (20)$$

This peak will rotate around the point (0.5, 0.5) in time. The boundary condition is  $u = 0$ . Although this is inconsistent with initial conditions it does not appear to lead to numerical difficulties.

The solution after one complete rotation is seen in Figure 3 in which both first and second order solutions are shown. The horizontal axis shows the variation in  $y$  for a fixed value of  $x=0.5$ . The mesh used consisted of  $100 \times 100$  uniform squares each subdivided into triangles. The peak is advected in a circular fashion without excessive smoothing. The points to note about the profiles are that there is no sign of undershoot or overshoot, although there is evidence of numerical diffusion for the low order scheme. The higher order scheme is much better at capturing the discontinuous profile of the advection front. This simple test case provides the confidence that the chosen numerical scheme can adequately represent the advection of steep solution gradients.

## 7 Plume dispersion including chemical transformations

The second test case describes the dispersion of a plume originating from a concentrated source of NO<sub>x</sub> such as a power station chimney (Tomlin et al, 1995). This problem includes nonlinear source terms generated by the chemical reaction rates and as such is a more difficult numerical test than the simple linear advection equation. The purpose of choosing such an application is to look at the multi-scale problem generated by the interaction of the power station plume with background air, and to compare the fully adaptive scheme described above with the size of mesh elements generally used in regional scale air pollution models. We have not used a detailed atmospheric model, but have simply chosen to represent the main features which would commonly be found in such a model, including slow and fast nonlinear chemistry, concentrated source terms, advection and diffusion.

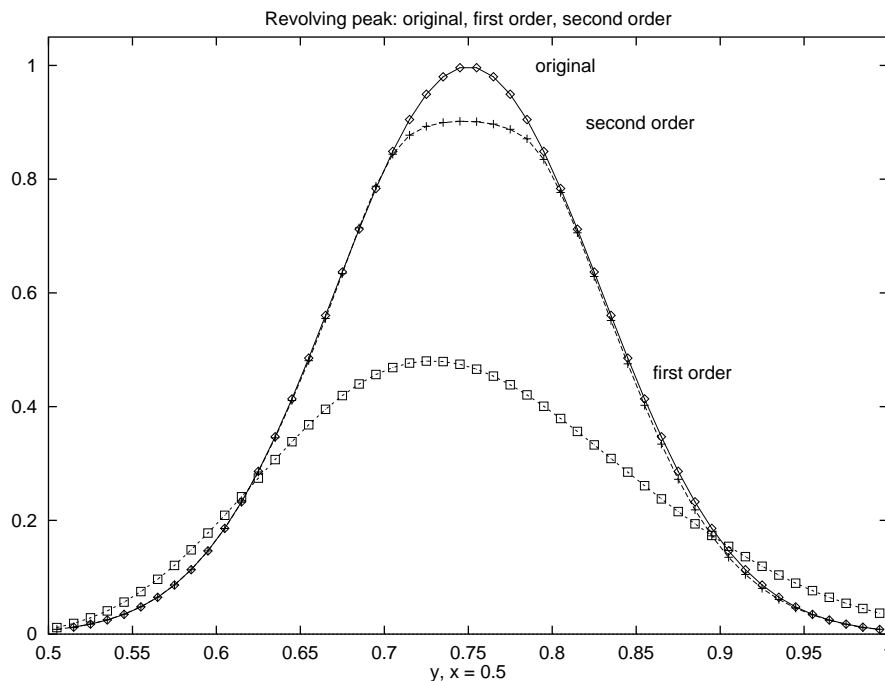
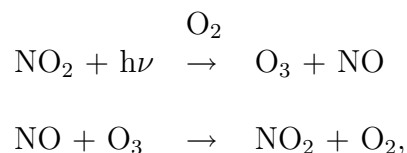


Figure 3: Results after one rotation for the Molenkamp problem for the first and second order schemes.

## 7.1 Chemical Mechanism

The simplified chemical mechanism used is shown in Table 1 and contains only 10 species. It therefore enabled fast turn around times with respect to developing the numerical code. Despite its simplicity it represents the main features of a tropospheric mechanism, namely the competition of the fast equilibrating inorganic reactions:



with the chemistry of volatile organic compounds (voc's), which occurs on a much slower time-scale. This separation in time-scales generates stiffness in the resulting equations. The voc reactions are represented by reactions of a single species, formaldehyde. This is unrealistic in terms of the actual emissions generated in the environment, but the investigation of fully speciated voc's is not the purpose of the present study. We therefore wished to include the minimum number of reactions which would lead to the generation of ozone at large distances from the NO<sub>x</sub> source. Deposition processes have not been included.

**Table 1**

	Reaction	Rate constant
$\text{NO}_2 + h\nu$	$\xrightarrow{\text{O}_2} \text{O}_3 + \text{NO}$	$a_1 = 1.45 \times 10^{-2}, b_1 = 0.4$
$\text{NO} + \text{O}_3$	$\rightarrow \text{NO}_2 + \text{O}_2$	$k_2 = 6.53 \times 10^{-11}$
$\text{O}_3 + h\nu$	$\rightarrow \text{O}^1\text{D} + \text{O}_2$	$a_3 = 2.0 \times 10^{-4}, b_3 = 1.4$
$\text{O}^1\text{D} + \text{H}_2\text{O}$	$\rightarrow 2\text{OH}$	$k_4 = 2.2 \times 10^{-10}$
$\text{OH} + \text{NO}_2$	$\rightarrow \text{HNO}_3$	$k_5 = 1.5 \times 10^{-11}$
$\text{OH} + \text{CO}$	$\rightarrow \text{CO}_2 + \text{H}$	$k_6 = 2.2 \times 10^{-13}$
$\text{H} + \text{O}_2 + \text{M}$	$\rightarrow \text{HO}_2 + \text{M}$	$k_7 = 5.1 \times 10^{-32} (\text{T}/300)^{-0.9}$
$\text{HO}_2 + \text{NO}$	$\rightarrow \text{NO}_2 + \text{OH}$	$k_8 = 8.3 \times 10^{-12}$
$\text{O}^1\text{D} + \text{M}$	$\rightarrow \text{O}_3$	$k_9 = 2.0 \times 10^{-11} e^{(100/\text{T})}$
$\text{HCHO} + \text{OH}$	$\rightarrow \text{HO}_2 + \text{CO} + \text{H}_2\text{O}$	$k_{10} = 1.0 \times 10^{-11}$
$\text{HCHO} + h\nu$	$\rightarrow 2\text{HO}_2 + \text{CO}$	$a_{11} = 3.32 \times 10^{-5}, b_{11} = 0.56$
$\text{HCHO} + h\nu$	$\rightarrow \text{H}_2 + \text{CO}$	$a_{12} = 5.54 \times 10^{-5}, b_{12} = 0.79$

The rate constants have been chosen to be in agreement with those used by Derwent et al. (1990) and are expressed as  $m^{\text{th}}$  order rate constants with units  $(\text{molecule cm}^{-3})^{1-m} \text{s}^{-1}$ . The photolysis rates were parametrised as a function of the solar zenith angle, giving a first order rate constant in the form:

$$J_i = a_i \exp(-b_i \sec\theta).$$

where  $i$  is the reaction number. The solar zenith angle  $\theta$  is calculated as a function of the time of day (given by the local hour angle LHA), the time of year (given by the solar declination angle DEC) and the latitude (LAT):

$$\cos(\theta) = \cos(\text{LHA}) \cos(\text{DEC}) \cos(\text{LAT}) + \sin(\text{DEC}) \sin(\text{LAT})$$

Temperature dependent rate constants were represented by a standard Arrhenius expression and the temperature calculated as function of time of day according to the following parametrisation;

$$T/K = 289.86 + 8.3\sin((7.27e-5t) - 1.96)$$

where t is the time in seconds. The concentration of H<sub>2</sub>O was also parametrised as follows:

$$RH = 66.5 + 23.0\sin((7.27 \times 10^{-5}t) + 1.18);$$

$$[H_2O] = 6.1078\exp(-(597.3 - 0.57(T - 273.16))18.0/1.986T - 1.0/273.16)(10.0RH)/(1.38e-16T);$$

where RH is the relative humidity and T the temperature.

The concentration of CO was taken to be a constant and was based on a background value of 120ppb. The concentration of oxygen was taken to be 20% of air at atmospheric pressure.

## 7.2 Background concentrations, source terms and transport parameters

The model was used to represent three separate scenarios of a plume of concentrated NO<sub>x</sub> emissions being dispersed through a background of clean and polluted air. The background concentrations listed in Table 2 formed the initial conditions for the model. Concentrations in the background change diurnally as the chemical transformations take place according to photolysis rates and temperature and concentration changes. Case A describes a situation where background voc's are high but the main source of NO<sub>x</sub> is the point source. This could represent for example a plume dispersing through a region of high biogenic emissions. Case B represents background air which is high in both voc and NO<sub>x</sub> concentrations. Case C represents a clean air situation where the background levels for NO<sub>x</sub> and voc's are low. The initial concentration of O<sub>3</sub> was the same for all scenarios. Background source terms were included for NO<sub>x</sub>, i.e. NO and NO<sub>2</sub> and formaldehyde. For the sake of simplicity the source term for formaldehyde is the same over all spatial points although it is possible to include unstructured emissions data by interpolation onto the triangular grid. We have not included such results here since we wish to highlight the effects of the mesh on the solution and therefore need to keep the physical problem fairly simple. The background source terms for formaldehyde and NO<sub>x</sub> were chosen so that the background concentration remained at the same order of magnitude.

**Table 2 - Initial conditions for background concentrations**

	A	B	C
NO <sub>2</sub> (molecule cm <sup>-3</sup> )	4.56 × 10 <sup>10</sup>	8.00 × 10 <sup>10</sup>	1.00 × 10 <sup>8</sup>
NO (molecule cm <sup>-3</sup> )	7.50 × 10 <sup>10</sup>	1.00 × 10 <sup>11</sup>	1.00 × 10 <sup>8</sup>
O <sub>3</sub> (molecule cm <sup>-3</sup> )	5.00 × 10 <sup>11</sup>	5.00 × 10 <sup>11</sup>	5.00 × 10 <sup>11</sup>
HCHO (molecule cm <sup>-3</sup> )	1.00 × 10 <sup>11</sup>	1.00 × 10 <sup>11</sup>	1.00 × 10 <sup>10</sup>

The power station was taken to be a separate source of NOx and this source was represented in a slightly different way. In this case the chimney region is treated as a subdomain and the concentration in the chimney set as an internal boundary condition. In terms of the mesh generation this ensures that the initial grid will contain more elements close to the concentrated emission source. This is similar in methodology to the telescopic approach. The concentration in the chimney corresponds to an emission rate of NOx of 400kg<sub>hr</sub><sup>-1</sup>. We have considered only 10% of the NOx to be emitted as NO<sub>2</sub>.

We have assumed a constant wind speed of 5ms<sup>-1</sup> in the x-direction. The eddy diffusion parameter was set at 300 m<sup>2</sup>s<sup>-1</sup> for all species.

### 7.3 Mesh generation and boundary conditions

The initial mesh was generated with only 100 elements. It is difficult to relate the size of unstructured meshes directly to regular rectangular ones, but our original mesh was comparable to the size of mesh generally used in regional scale atmospheric models, the largest grid cell being approximately 60km along its longest edge. Close to the chimney the mesh was refined to elements of length 5km ensuring that it would be refined to a reasonable resolution in this region of steep gradients. If we allow the mesh to refine two levels then the smallest possible mesh size close to the chimney will be 1.25km in length. Spatial errors in the concentration of NO were chosen as the criterion from which to further refine the mesh. Test runs showed that regions of high spatial error coincided with steep spatial gradients. The mesh can therefore be considered to adapt around steep NO concentration gradients.

## 8 Results

Each run was carried out over a period of 48 hours starting from midnight on day 1, so that the diurnal variations could be observed. We present here only a selection of the results which illustrate the main features relating to the adaptivity.

Figure 4 compares the structure of the base mesh with a mesh which has been adapted up to level 2 at 14.00 on day 2. In this figure the sides of the polygons represent the

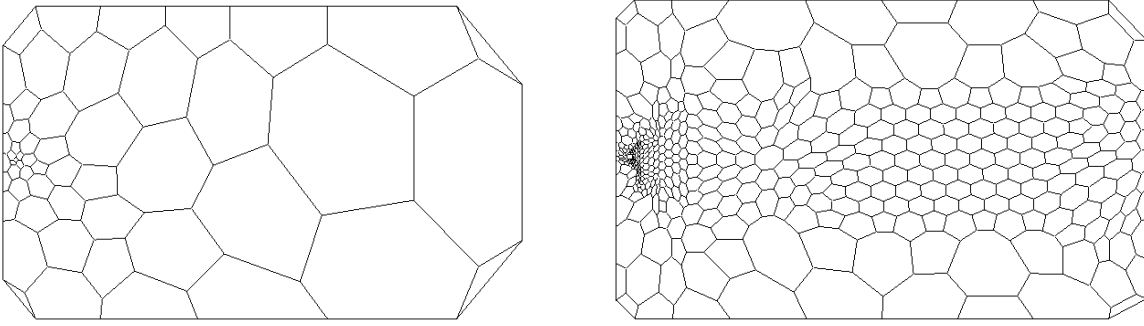
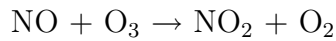


Figure 4: The structure of the level 0 and level 2 adaptive mesh. The length of the domain is 300km and the width 200km. The smallest and largest mesh lengths are approximately 5 and 60km respectively for the level zero domain.

distance between cell centres on the triangular mesh. We can see that the main area of mesh refinement is along the plume edges close to the chimney, indicating that there is a high level of structure in these regions. Figure 5 shows the  $O_3$  concentrations in ppb for the level 0 and level 2 meshes for case A at 14.00 on day 2. On the coarse mesh the plume is dispersed over a much larger area than on the fine mesh and most of the plume structure is lost. Close to the stack the concentration of  $O_3$  is much lower than that in the background because of high  $NO_x$  concentrations. The inorganic chemistry is dominant in this region and the ozone is consumed by the reaction:



As the plume travels downwind and the  $NO_x$  levels decrease, the plume gradually mixes with background voc's leading to the production of  $NO_2$  which reverses the above reaction. The concentrations of ozone can therefore rise above the background levels at quite large distances downwind from the source of  $NO_x$ . The peak ozone concentrations which occur at the plume edges in the level 2 calculation are not captured by the level 0 solution.

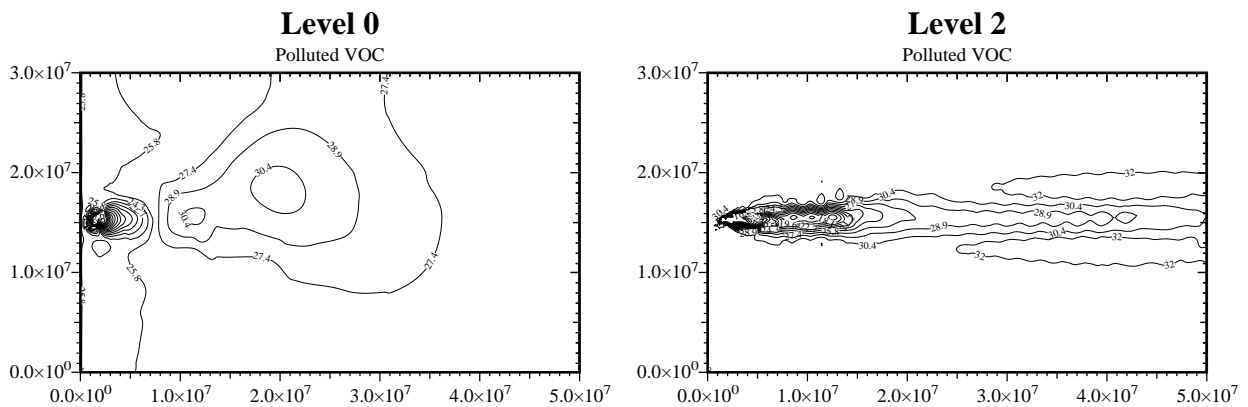


Figure 5: Ozone contours for case A, voc polluted air, level 0 and level 2 calculations. Concentrations are in ppb.

In figure 6 we present a cross plume profile of the  $\text{NO}_2$  concentrations at a distance of 10km downwind of the chimney stack for case A at the same time as the previous figure. The figure clearly shows the features at the edge of the plume which are revealed by the adaptive solution. From the base mesh, where the distance between elements along the y-axis close to the stack is 20km, it appears that the concentration of  $\text{NO}_2$  rises to a peak in the centre of the plume. If the mesh is refined to higher levels then we start to see the true structure of the plume emerging. With a level 3 solution we can see that the peak concentrations are actually found along the edges of the plume and that the concentration of  $\text{NO}_2$  drops to very low levels at the plume centre. From the area under these curves it is found that there is a 30% difference between the overall level 0 and the level 3 concentrations. This shows that not only the peak concentrations, but the total integrated concentrations are very different for the different levels of adaptivity. It is clear therefore that using a very coarse grid in regions of steep spatial gradients can lead to an over estimate of total pollutant concentrations.

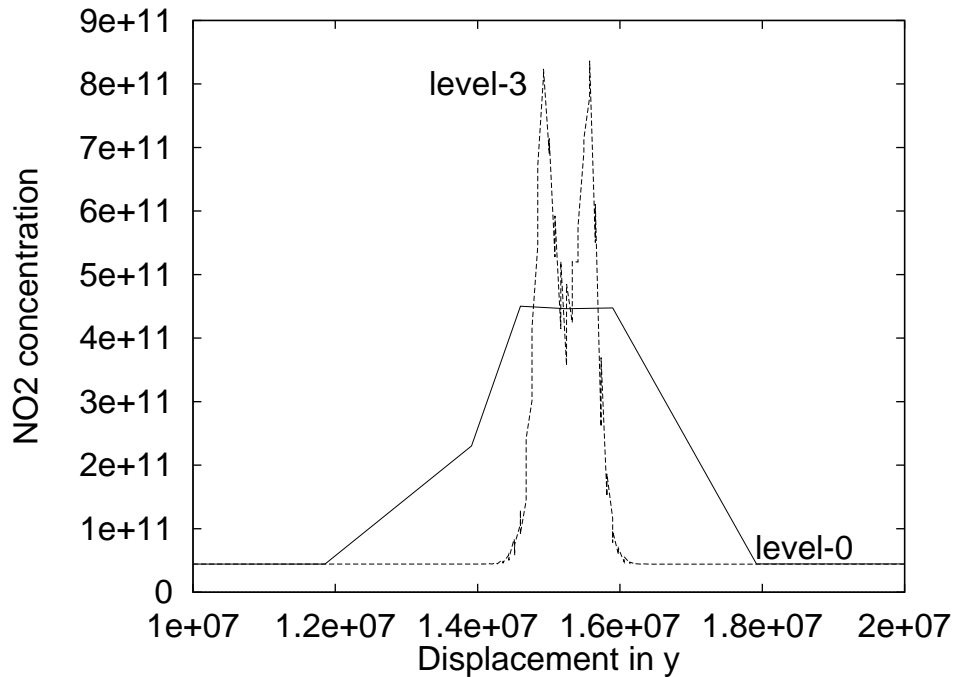


Figure 6: Cross plume  $\text{NO}_2$  profiles 10km from stack in molecules  $\text{cm}^{-3}$ , showing how the level 3 solution captures the structure of the plume.

Figure 7 shows the  $\text{O}_3$  concentration for case B again at 14.00 on day 2, and Figure 8 for case C. In both cases the plume is over-dispersed in the level 0 case and the spatial distribution of ozone is therefore inaccurately represented. In case B, polluted air, the ozone concentrations in the level 2 solution drop quite significantly at the plume centre. For the level 0 solution there is a large degree of smearing out of the concentrations and the plume centre concentrations do not drop too far below the background levels. Again for case C, the clean air case, the levels of ozone drop considerably in the plume compared to the background since the levels of  $\text{NO}$  are much higher there. For the level 0 case these lowered concentrations spread over very large distances owing to the over-dispersion of the plume. The location of reduced/raised concentrations will therefore be incorrect for the level 0 results in all three

cases. For each scenario the level 0 solution leads to a smoothing out of the ozone profiles so that the true structure caused by the interaction of the plume with background air is missed.

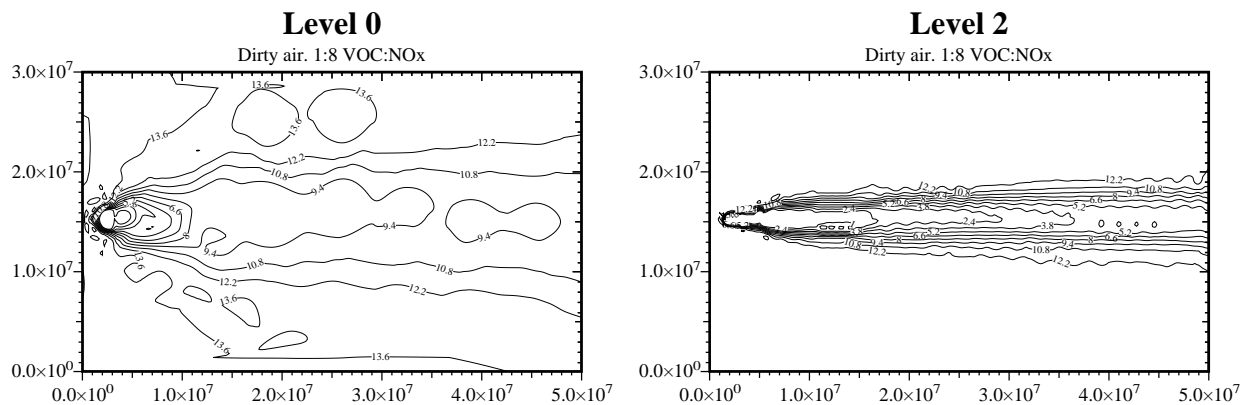


Figure 7: Ozone contours for case B, polluted air, level 0 and level 2 calculations.

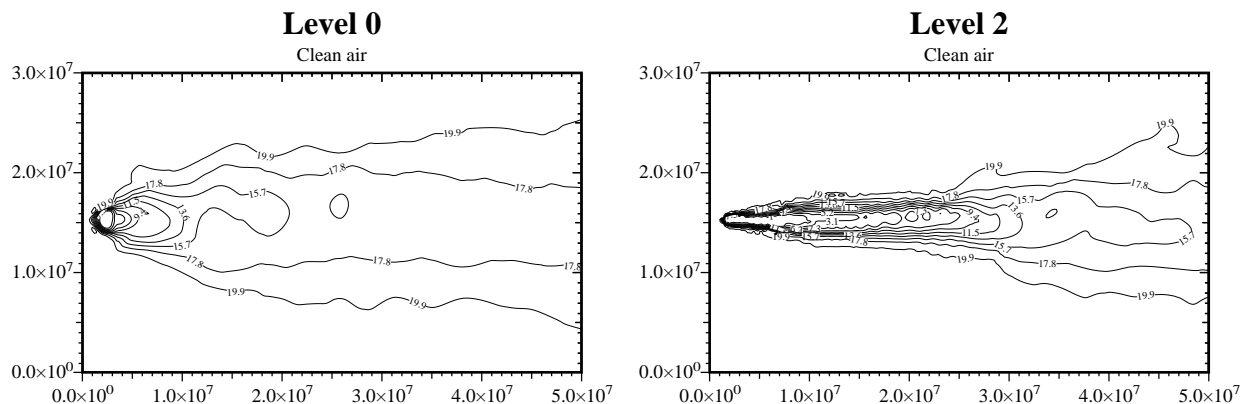


Figure 8: Ozone contours for case C, clean air, level 0 and level 2 calculations.

## 9 Discussion

We have shown above that there are key features of plume characteristics which cannot be represented by the coarse meshes generally used in regional scale models. Steep concentration gradients close to the stack, such as the the variations in  $\text{NO}_2$  concentrations, might be captured by telescopic models which provide a higher resolution in concentrated emission areas. However, features such as the peak ozone concentrations which occur at the edges of the plume for a long distance downwind of the source, may not be captured by such techniques. For example, there is a strong possibility that peak ozone levels will occur in low emission regions such as rural areas. Telescopic models would not refine in such low emission regions and a fully adaptive algorithm might be the best way to resolve such features at large distances downwind from the source. Since the adaptive method changes according to only

the current solution rather than in a prescribed way, the grid should be able to cope with changing wind conditions as well as refining according to source patterns. This application needs to be tested in future work.

We have also indicated that as well as inaccurately describing peak concentrations and concentration profiles, coarse meshes can also lead to inaccurate estimates of average or integrated concentration levels. This is important if we are to use models to predict total budgets for individual species. One of the key reasons why such errors might appear is the nonlinearity in the chemical reaction rates. The nonlinear dependency of ozone concentrations on NO<sub>x</sub> has been discussed many times in the literature and is well understood (Liu et al, 1987). Sillman et al (1990) have also discussed the interaction between the computational mesh and nonlinear ozone chemistry, and have demonstrated the errors which can occur due to using a coarse mesh in regions where plumes exist. Unless we are refining to very high levels the nonlinear chemistry will be mesh dependent. Since it is impossible in atmospheric models to reach a level of refinement where full convergence can be achieved, then this will almost certainly be true in some regions of the model, particularly regions where steep gradients occur.

For example, consider the simple nonlinear reaction



If we compare the value of the rate of this reaction  $k[A][B]$  for a single element and an element which has been adapted into four subelements, we can see that the total rates for the two cases will not be equal. The concentrations of A and B in the large element are assumed to be the average of that in the four smaller elements:

$$A_{\text{avg}} = \frac{1}{4} \sum A_i \quad i = 1,2,3,4$$

$$B_{\text{avg}} = \frac{1}{4} \sum B_i \quad i = 1,2,3,4$$

The source terms for the large element can now be evaluated as:

$$\text{rate} = k A_{\text{avg}} B_{\text{avg}} = k \frac{1}{4} \sum A_i \frac{1}{4} \sum B_i$$

For the four smaller elements we take the source terms to be the average of the rates in each element:

$$\text{rate} = k/4 \sum (A_i B_i)$$

The above two expressions will only be close in value if the concentrations in each of the four cells are almost equal, so that for regions of steep spatial gradient there are likely to be large errors induced by the nonlinear terms.

## 10 Conclusions

We have presented in this work a simple example in order to illustrate the potential importance of adaptive methods for the solution of atmospheric models. Using a case study of a power station plume we have illustrated the need for adaptive methods in order to accurately represent the interaction of a concentration pollution source with background levels. The adaptive solution reveals features such as peak levels of  $\text{NO}_2$  and  $\text{O}_3$  which could not be detected using a coarse mesh. The change in mesh refinement also resulted in a change in overall or integrated concentration levels. This indicates that due to strongly nonlinear terms in the chemical reaction rates, the source terms in the p.d.e. will be mesh dependent. Without using a fine mesh over the whole domain so that the concentrations in neighbouring cells differ only very little, the effects of this nonlinearity could be quite significant. To reduce the effects it is important to refine the mesh at least in regions of steep spatial gradients. This has been partially addressed by the telescopic methods presently used in air quality models. However, the present test case has shown that steep gradients can occur at long distances downwind from the source, for example the change in ozone concentrations along the edges of the plume. Adaptive algorithms seem to present a successful method of achieving accuracy in such regions and can do so in an automatic way.

The work here is fairly preliminary in terms of using adaptive methods in a full air pollution model. Questions of whether adaptivity is necessary in the vertical direction and whether to use structured or unstructured meshes have still to be answered and the authors intend to address these questions in their future work.

**Acknowledgements** The authors would like to thank the CEC for funding AST and JS and Anne Heard for helpful discussions.

## References

- Berzins M., Gaskell P.H., Sleigh A., Speares W., Tomlin A. and Ware J.M., An Adaptive CFD Solver for Time-Dependent Environmental Flow Problems, *proc of ICFD Conference on Numerical Methods in Fluid Dynamics*, Eds K.W. Morton and M.J. Baines to appear
- Berzins M., Dew P.M., and Furzeland R.M. (1989) Developing software for time-dependent problems using the method of lines and differential algebraic integrators. *Appl. Numer. Math.*, , 5375-390.
- Berzins M., Lawson J., and Ware J. (1992) Spatial and Temporal Error Control in the Adaptive Solution of Systems of Conservation Laws, In R. Vichnevetsky, D. Knight, and G. Richter, editors, *Advances in Computer Methods for Partial Differential Equations VII*, IMACS, 60-66.
- Berzins M. and Ware J.M. (1994). Reliable Finite Volume Methods for the Navier Stokes Equations. *Notes on numerical Fluid Mechanics* (Eds) F-K Hebeker, R.Rannacher and G.Wittum, Viewg, Wiesbaden, **47**, 1-8.
- Berzins M. (1994) Temporal Error Control in the Method of Lines for Convection Dominated p.d.e.s. *SIAM J. Sci. Comp.***16**, 558-580.
- Berzins M. and Ware J.M. (1995) Positive cell-centered finite volume discretization methods for hyperbolic equations on irregular meshes. *Appl. Num. Math.* , **16**, 417-438.
- Berzins M. and Ware J.M. (1996). Solving Convection and Convection-Reaction Problems using M.O.L. *Appl. Num. Math. to appear* .
- Chock D.P. (1991) A comparison of numerical methods for solving the advection equation III. *Atmos. Env.* , **25A**, 553-571.
- Derwent R. G. and Jenkin M.E. (1990) *Hydrocarbon involvement in photochemical ozone formation in Europe* AERE-report-R13736
- Jakobs H.J. (1994) *Eurotrac94 - ISS Garmisch-Partenkirchen*
- Joe B. and Simpson R.B. (1991) Triangular meshes for regions of complicated shape, *Int. J. Numer. Meth. Eng.* **23**, 987-997.
- Liu S.C., Trainer M., Fehsenfeld F.C., Parrish D.D., Williams E.J., Fahey D.W., Hubler G., and Murphey P.C. (1987) Ozone production in the rural troposphere and the implications for regional and global ozone distributions *J. Geophys. Res.* **92**, 4191-4207.
- Peters L.K., Berkovitz C.M., Carmichael G.R., Easter R.C., Fairweather G., Ghan S.J., Hales J.M., Leung L.R., Pennell W.R., Potra F.A., Saylor R.D. and Tsang T.T. (1995) The current and future direction of Eulerian Models in simulating the tropospheric chemistry and transport of trace species: a review *Atmospheric Environment***29** 189-222.

- Molenkamp C.R. (1968) *J.Appl. Meteorol.* **7**, 7.
- Moussiopoulous N. (1994) The EUMAC zooming model *Eurotrac94 - ISS Garmisch-Partenkirchen*
- Sillman S., Logan J. A., Wofsy S. C. (1990) *J. Geophys. Res.* **95**, 1837
- Skamarock W., Olinger J. and Street R.L. (1989) Adaptive Grid Refinement for Numerical Weather Prediction. *Journal of Computational Physics*, **80**, 27-60.
- Spekreijse S. (1987) Multigrid solution of monotone second order discretizations of hyperbolic conservation laws. *Math. Comp.*, **47(179)** , 135-155.
- Sunderam S., Logan J.A. and Wofsy. S.C. (1990) A Regional Scale Model for Ozone in the United States With Subgrid Representation of Urban and Power Plant Plumes. *Journal of Geophysical Research*, **95**, 5731-5748.
- Tomlin A.S., Pilling M.J., Heard A. (1994) Emissions of radiative gases and ozone precursors from coal use. Progress Report No 1, Contract No JOU-CT92-0229, Joule 2 Program, C. E. C.
- Tomlin A., Ware J., Smith J., Berzins M., Pilling M.J. (1995) Efficient high resolution methods for air pollution models, *Air Pollution III - Computational Mechanics special publication*, 201-209.
- VanLoon M. (1996) Numerical methods in smog prediction. *PhD. Thesis*, GWI Amsterdam.
- Verwer J.G. (1994) Gauss Seidel Iteration for Stiff o.d.e.s from Chemical Kinetics. *SIAM J. Sci. Comp* , **15**, 1243-1250.
- Vreugdenhil C. B. and Koren B. (1993) Numerical methods for advection-diffusion problems. *Notes on numerical fluid mechanics* , bf 45, Vieweg, Braunschweig/Weisbaden, ISBN 3-528-07645-3.
- Ware J. and Berzins M. (1995) Adaptive Finite Volume Methods for Time-dependent P.D.E.s. , Modeling, Mesh Generation and Adaptive Numerical Methods for PDEs.(Eds.) I. Babuska et.al. Volume 75 in IMA Volumes in Mathematics and Its Applications Series, Springer Verlag, 417-430